



A comprehensive numerical model for the thermodynamic and transport properties of H₂O-NaCl fluids

Yury I. Klyukin^{a,b,*}, Erik L. Haroldson^c, Matthew Steele-MacInnis^a

^a Department of Earth and Atmospheric Sciences, University of Alberta, 1-26 Earth Sciences Building, Edmonton, AB T6G2E3, Canada

^b Department of Geoscience, University of Calgary, Earth Science, 2500 University Dr. NW, Calgary, AB, T2N1N4, Canada

^c Department of Geosciences, Austin Peay State University, P.O. Box 4418, Clarksville, TN 37044, United States of America

ARTICLE INFO

Editor: Donald Dingwell

Keywords:

Fluid phase equilibria
Mineral solubility
Fluid inclusions
H₂O-NaCl
Salinity
Hydrothermal fluids
Microthermometry

ABSTRACT

Saline fluids are common to a variety of geologic settings in Earth's crust and upper mantle. The binary system H₂O-NaCl is commonly used to interpret data obtained from fluid inclusions, and for geochemical modeling of mass and energy transport and fluid-rock interaction. Modeling of fluid properties in this binary system has generally relied on piecemeal compilations from available models specific to certain properties, whereas a standalone, comprehensive tool has been lacking. Here, we present a new computer package, entitled *ProBrine* (Properties of Brine) to evaluate the thermodynamic and transport properties of H₂O-NaCl fluids over the range of temperatures from 0 to 1000 °C, pressure from 1 to 5000 bar, and salinity from 0 to 100 wt% NaCl. *ProBrine* is designed to calculate a wide range of thermodynamic and transport properties, including (but not limited to): phase equilibria (liquid, vapor, and halite); molar volume, density, specific enthalpy, and viscosity. The program is also equipped to calculate derived properties such as: 1) the coefficient of isobaric thermal expansion; 2) the coefficient of isothermal compressibility; 3) the reduced susceptibility; 4) the isobaric specific heat capacity, and the fluxibility. In addition, the model will calculate solubility of the following six minerals: fluorapatite, calcite, corundum, fluorite, rutile, and quartz, as well as the respective temperature and pressure derivatives, which can be used to predict mineral dissolution and precipitation along a flow path. Moreover, the program is equipped to interpret fluid-inclusion data. The program is written in Visual Basic (VBA) in Microsoft Excel and is released open-source, allowing a user full scope to review, copy, modify and expand the program code.

1. Introduction

Geologic fluids in many settings are multicomponent solutions that include H₂O plus a variety of dissolved components (Roedder, 1972, 1984; Kesler, 2005). Saline aqueous geologic fluids are commonly represented by simplified and well-characterized binary or ternary systems in geochemical modeling. These binary and ternary systems include various electrolytes (KCl, CaCl₂, MgCl₂) combined with H₂O (Steele-MacInnis et al., 2016). For example, widely used model chemical systems include H₂O-NaCl-CaCl₂ (Steele-MacInnis et al., 2011); H₂O-NaCl-FeCl₂ (Lecumberri-Sánchez et al., 2015); H₂O-NaCl-KCl (Lecumberri-Sánchez et al., 2020); and H₂O-NaCl-CO₂ (Steele-MacInnis, 2018; Li et al., 2020). For a detailed review of thermodynamic models available for other geologically relevant chemical systems, the reader is referred to Gottschalk (2007). Still, the most widely applicable and commonly used binary system used for representing hydrothermal fluids in geologic settings is H₂O-NaCl (Steele-

MacInnis et al., 2012b; Klyukin et al., 2019).

The H₂O-NaCl system has been the subject of intensive characterization in terms of physical and chemical properties (Bodnar et al., 1985; Bischoff and Rosenbauer, 1988; Mao and Duan, 2009), and numerous numerical models (Anderko and Pitzer, 1993; Palliser and McKibbin, 1998a, 1998b, 1998c; Driesner, 2007; Driesner and Heinrich, 2007) and associated computer packages (Bowers and Helgeson, 1983; Driesner, 2007; Steele-MacInnis et al., 2012b; Bakker, 2018, 2019) have been released to evaluate and interpret fluid properties in this system. Application of these models has revealed a variety of key consequences of considering the multicomponent nature of geologic fluids, compared to simpler models based exclusively on the single component H₂O: 1) for interpretation of data from fluid inclusions, salinity strongly affects estimation of density and isochore (Driesner, 2007), and the H₂O system is categorically insufficient to explain, for example, inclusions that homogenize at temperatures greater than the critical point of H₂O (Klyukin et al., 2016); 2) in

* Corresponding author at: Department of Geoscience, University of Calgary, AB, Canada.

E-mail address: Yury.Klyukin@ucalgary.ca (Y.I. Klyukin).

theoretical modeling of hydrothermal systems, such as those at mid-ocean ridges, incorporation of salinity has key consequences that explain, for example, the maximum observed temperatures achieved in these systems (Jupp and Schultz, 2004; Coumou et al., 2008); 3) for hydrodynamic modeling of, for example, magmatic-hydrothermal systems, salinity has key consequences for fluid flow patterns and fluid phase equilibria (Weis et al., 2014; Weis, 2015); 4) for modeling fluid-rock reactions, salinity has key consequences for activities, chemical reactivity, and obvious effects on reactions such as alkali exchange (Miron et al., 2016; Frank et al., 2003); and 5) for reactive transport modeling, salinity has key consequences for where and how minerals are precipitated or dissolved (Steele-MacInnis et al., 2012a; Monecke et al., 2018). Thus, numerical models that can be used to quantify these phenomena are valuable to characterizing and interpreting a wide variety of geologic processes.

At present, several models are available to calculate various subsets of thermodynamic and transport properties of H₂O-NaCl fluids, but no single available computer package explicitly links these properties in one program that can be used to run simulations and/or interpret large datasets. Currently, existing programs are based on formulations (equations of state, EoS) for phase equilibria and transport or physical properties of H₂O-NaCl. Most notable of those is the fundamental EoS of Anderko and Pitzer (1993), and empirical EoS of Bowers and Helgeson (1983), Palliser and McKibbin (1998a, 1998b, 1998c), Driesner (2007), and Driesner and Heinrich (2007). To date, the most accurate reproduction of the experimental data is achieved by the model of Driesner and Heinrich (2007) for phase equilibria of H₂O-NaCl and Driesner (2007) for density, enthalpy, and isobaric heat capacity. The fundamental EoS formulation of Anderko and Pitzer (1993) provides a wide range of thermodynamic properties, but in its current status is limited to temperatures above 300 °C, and it reproduces experimental data with less accuracy than those of Driesner (2007) and Driesner and Heinrich (2007).

Numerous existing programs have been designed to interpret fluid inclusions measurements, phase equilibria and/or fluid properties of H₂O-NaCl composition, including but not limited to: MacFlinCor (Brown and Hagemann, 1995), the model and EoS developed by Duan et al. (1995), SoWat, (Driesner, 2007; Driesner and Heinrich, 2007), HokieFlincs (Steele-MacInnis et al., 2012b) and AqSo_NaCl (Bakker, 2018, 2019). MacFlinCor and the model by Duan et al. (1995) are currently unsupported. SoWat provides little functionality to interpret data from fluid inclusions and to evaluate fluid phase equilibria, density, and isobaric heat capacity. HokieFlincs is focused solely on interpretation of data from fluid inclusions. AqSo_NaCl is capable of evaluating fluid properties at specific PTx conditions or fluid inclusion properties.

In the present study, we describe a new computer package, entitled *ProBrine* (Properties of Brine), that incorporates a comprehensive and internally consistent set of numerical models, in order to comprehensively describe the properties of H₂O-NaCl from 0 to 1000 °C, 1 to 5000 bar, and 0 to 100 wt% NaCl. The model has been designed to be deliberately generic, allowing the user complete flexibility to decide the input and output parameters and ranges of physical conditions to explore. Below, we first briefly describe the phase equilibria and fluid properties of the H₂O-NaCl system, then describe their incorporation into the program *ProBrine*.

2. Phase equilibria and fluid properties of H₂O-NaCl

In the following subsections, we briefly introduce some of the key properties of H₂O-NaCl fluids that can be modeled using the program described here. For each property, we also list the selected numerical models that have been incorporated in the program.

2.1. Phase equilibria

The single-component system H₂O is characterized by three univariant lines along which solid-vapor, solid-liquid, and liquid-vapor phases can coexist in equilibrium. These lines intersect at a triple point, where solid, liquid and vapor are in equilibrium. The triple point in the system H₂O occurs at 0.01 °C and 0.006 bar, and is the point of origin of the liquid-vapor coexistence line that terminates at the critical point at 373.946 °C and 220.64 bar (Wagner and Prüß, 2002). At temperatures and pressures above the critical point, H₂O is a single-phase “super-critical” fluid. The system H₂O is sometimes used as a simplified substitute for geologic fluids in numerical models (Norton, 1984; Garven, 1985; Jupp and Schultz, 2000, 2004) owing to its well-characterized properties and phase equilibria, but it must be stressed that this simplified approach will commonly fail to capture important phenomena such as phase separation at temperatures exceeding 373.946 °C or at pressures above or below the H₂O boiling curve.

Two-component systems are characterized by significantly different topologies of the phase diagram, compared to a single component system like H₂O, and the specific topology of a binary system depends on the chemical similarity between the two components (Valyashko, 2008). The system H₂O-NaCl falls in the “Type 1” category of binary systems (Valyashko, 2008) and is thus characterized by a continuous critical curve that extends from the critical point of H₂O to that of NaCl (Fig. 1, green line; Fig. 2A and B; Liebscher and Heinrich (2007)). This system is also characterized by a continuous vapor-saturated solubility curve (or three-phase curve) that extends from the triple point of H₂O to that of NaCl. At pressures below the three-phase curve lies the stability field of vapor + halite. Between the critical curve and the three-phase curve, is a two-phase field of liquid + vapor immiscibility. A halite liquidus surface extends from the three-phase curve to higher pressure, and separates the single-phase fluid field at higher temperatures and lower salinities, from a two-phase liquid + halite field at lower temperatures and higher salinities (Fig. 1). The single-phase fluid field can be further subdivided into fields of “liquid-like” fluid (higher density, herein referred to as liquid) and “vapor-like” fluid (lower density, herein referred to as vapor) by a surface defined by the locus of critical isochores. Note that the latter is not a phase boundary, and there is no discontinuity in properties of liquid versus vapor in the single-phase field.

In the present work, we evaluate phase equilibria in the H₂O end-member system using the IAPWS-95 equation of state of Wagner and Prüß (2002). For the H₂O-NaCl binary system, we use the empirical model of Driesner and Heinrich (2007). Note that the latter model was originally based on the earlier IAPWS-84 formulation of Haar et al. (1984). We performed extensive testing of the H₂O-NaCl formulation using both the IAPS-84 and IAPWS-95 equations, and found that they yielded only negligible differences in terms of phase equilibria and density, even at extremely low salinities.

2.2. Thermodynamic properties

2.2.1. Base thermodynamic properties

The EoS for properties of H₂O-NaCl (Driesner, 2007) provides a formulation to calculate density and enthalpy. Density quantifies the mass of the fluid in a given volume, while enthalpy is a measure of the thermal energy of the system.

2.2.2. Derived thermodynamic properties

Isobaric heat capacity is the enthalpy derivative with respect to temperature at constant pressure. Heat capacity quantifies the ability of a fluid to obtain/release heat energy. Density derivatives with respect to pressure at constant temperature (isothermal compressibility β) and with respect to temperature at constant pressure (isobaric expansion α) quantify the ability of a fluid to transport mass. Density- and enthalpy-derived parameters change non-linearly in PTx space; at specific PTx

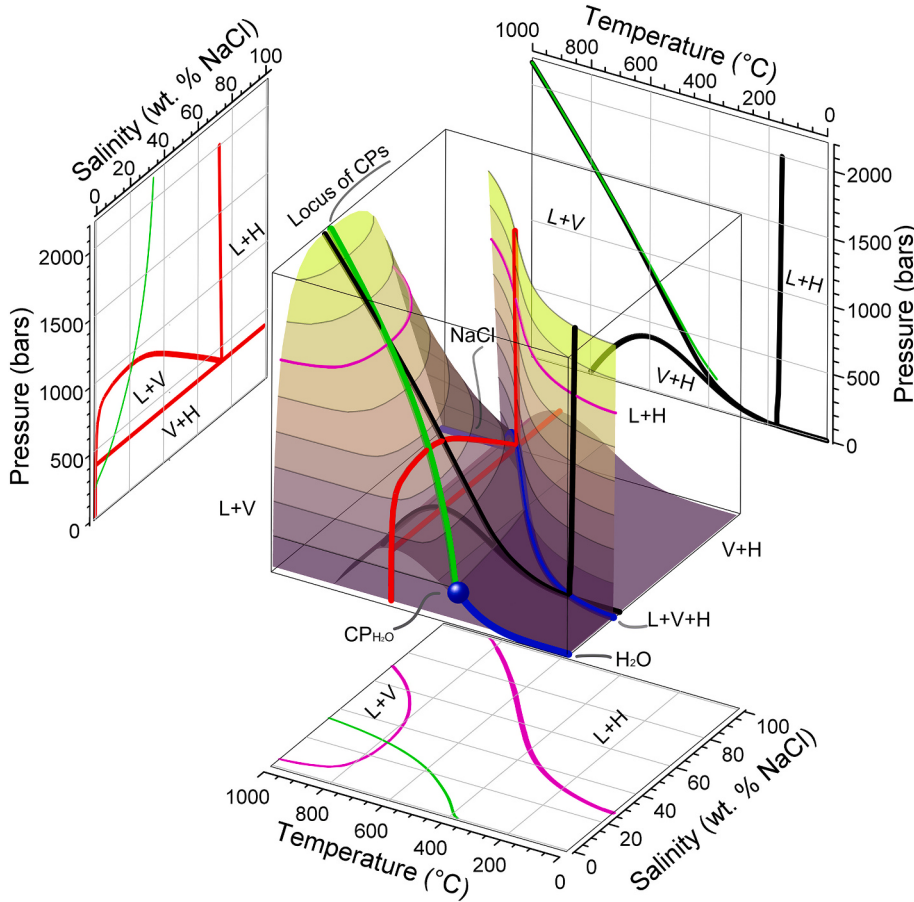


Fig. 1. Pressure-temperature-composition phase diagram for $\text{H}_2\text{O}-\text{NaCl}$ showing liquid + vapor ($\text{L} + \text{V}$), liquid + halite ($\text{L} + \text{H}$), vapor + halite ($\text{V} + \text{H}$) coexisting surfaces (colored semi-transparent surfaces with tie lines every 250 bar), boiling curve for water and pure NaCl , curve of coexisting liquid + vapor + halite ($\text{L} + \text{V} + \text{H}$) (blue lines) locus of $\text{H}_2\text{O}-\text{NaCl}$ critical points (green line) and critical point for pure H_2O . Black lines indicate cross section at constant salinity of 30 wt% NaCl . Magenta colored lines show isobaric cross section at 1500 bar. Red lines indicate isothermal cross section at 600 °C. Projections of the cross sections and locus of critical points are shown on the sides. Detailed description of functions used to create cross sections and 3D diagrams is provided in the text. (For interpretation of the references to color in this figure legend, the reader is referred to the web version of this article.)

conditions, $\text{H}_2\text{O}-\text{NaCl}$ fluids demonstrate rapid change in a list of properties in a response to minor changes in pressure, temperature or composition. Such PT_x conditions, referred to as the “critical region” and sometimes “supercritical region,” can be identified following the approach outlined by Anisimov et al. (2004). The latter approach is based on the derived parameter of reduced susceptibility factor ($\tilde{\chi}$), the value of which is used to identify PT limits of the critical region. While the susceptibility factor is defined as a partial derivative of the density with respect to chemical potential at constant temperature, the *reduced* susceptibility factor is defined as a function of density, isothermal compressibility, critical pressure and critical density. A detailed analysis of the mass and energy transport properties of a fluid, as well as a complete description of aforementioned derivatives, is provided in Klyukin et al. (2016).

2.3. Transport properties

The fluxibility parameter (F) quantifies the buoyancy-controlled ability of a fluid to transport heat. This parameter, introduced by Lister (1995), is used to illustrate that a pure H_2O fluid reaches maximum F at approximately 400 °C and 300 bar (Jupp and Schultz, 2000, 2004; Coogan et al., 2019). Application to a $\text{H}_2\text{O}-\text{NaCl}$ fluid (Klyukin et al., 2016) demonstrates that a low-salinity fluid is more efficient in transporting heat in buoyancy driven conditions.

Fundamental models for the dynamic viscosity of the $\text{H}_2\text{O}-\text{NaCl}$ system are lacking due to the complex nature of the viscosity property itself, and only empirical models have been developed. EoS for the dynamic viscosity of $\text{H}_2\text{O}-\text{NaCl}$ in most of the cases have limited range in temperature, pressure or composition. The only empirical EoS for $\text{H}_2\text{O}-\text{NaCl}$ dynamic viscosity, that would operate in wide range of PT_x conditions, are those of Palliser and McKibbin (1998c) and Klyukin

et al. (2016). We refer to the work of Klyukin et al. (2016) for a review of existing viscosity formulations and their comparison. In the present work we adopted this model, as it reproduces experimental data well and follows expected trends in PT_x ranges not covered by experimental data.

2.4. Mineral solubility

For the mineral solubility, we implemented the model of Akinfiev and Diamond (2009) for quartz, and that of Brooks and Steele-MacInnis (2019) for quartz, calcite, corundum, fluorapatite, fluorite and rutile.

2.5. Properties determined from fluid-inclusion data

Characterization of the compositions, densities and other properties of saline aqueous fluids in geologic settings is commonly done using fluid inclusions – aliquots of fluid trapped within a mineral during its growth or later crack healing (Roedder, 1984). Compositions of fluid inclusions are most commonly estimated by microthermometry, in which the temperatures of phase transitions are measured. The interpretation of microthermometric data, in terms of compositions and other properties, relies on equations of state for the fluid. For example, in a fluid inclusion of $\text{H}_2\text{O}-\text{NaCl}$ composition, the NaCl content is identified by melting temperature (i.e., temperature of disappearance) of ice, halite or hydrohalite. Similarly, the homogenization temperature (temperature of the phase transition from coexisting liquid and vapor phases ($\text{L} + \text{V}$) to single phase fluid, either liquid or vapor) is used to estimate the bulk density and molar volume of the fluid.

While most of the properties necessary for fluid inclusion characterization directly arise from volumetric properties (density) and equation of state modeling (pressure at homogenization), salinity

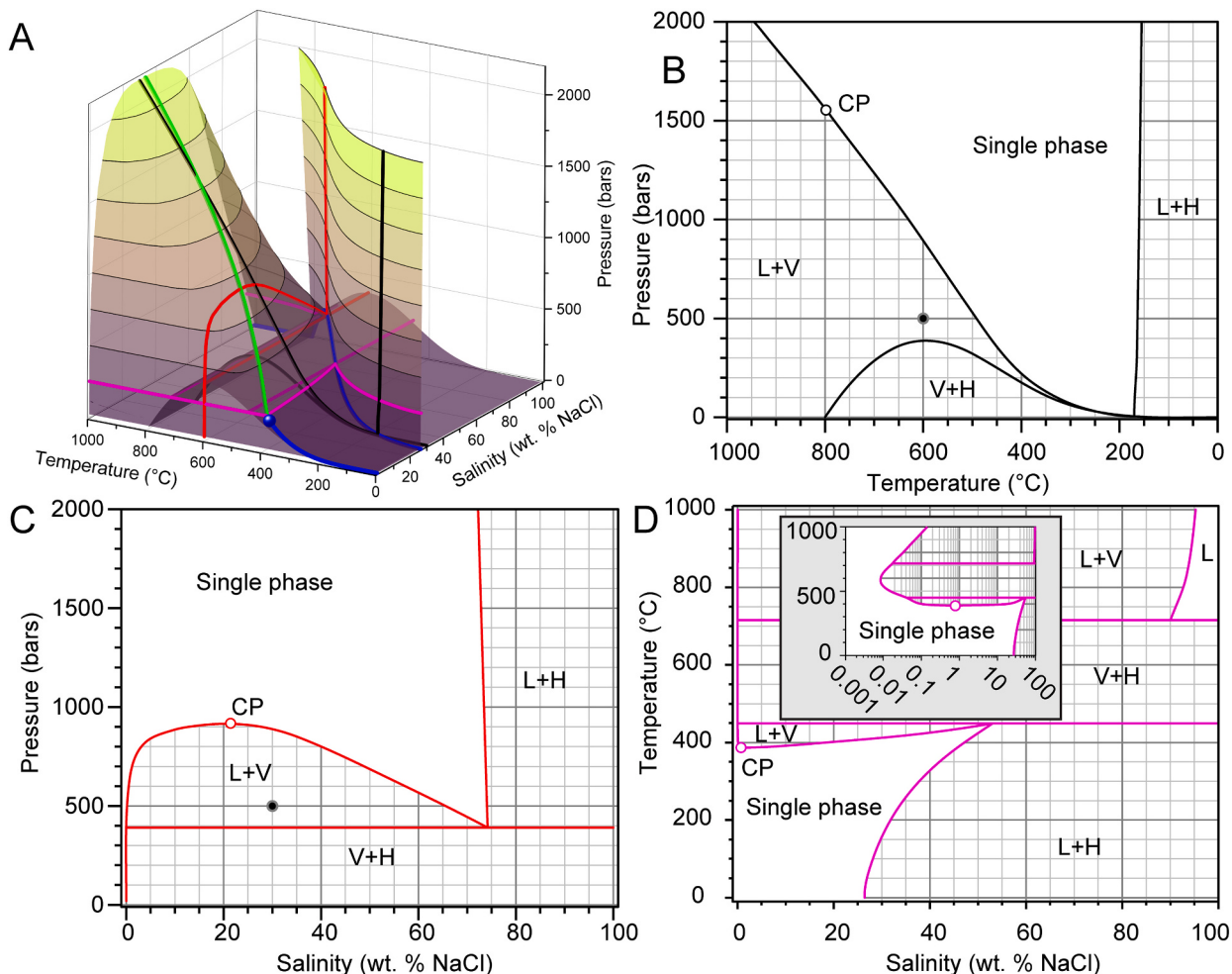


Fig. 2. A. Pressure-temperature-composition phase diagram for H_2O -NaCl showing liquid + vapor ($\text{L} + \text{V}$), liquid + halite ($\text{L} + \text{H}$), vapor + halite ($\text{V} + \text{H}$) coexisting surfaces, boiling curve for water and pure NaCl, curve of coexisting liquid + vapor + halite ($\text{L} + \text{V} + \text{H}$), locus of critical points and critical point for pure H_2O . B. A cross section at 30 wt% NaCl; C. A cross section at 600 °C; D. A cross section at 250 bar, inset shows this cross section with log-scale salinity.

interpretation relies on empirical models that correlate observed phase transition temperature with concentration of NaCl in solution. In the present study, we combined the following empirical models for salinity identification:

- For ice melting, the model of Bodnar (1993);
- For hydrohalite dissolution, and for halite dissolution at temperatures less than the liquid-vapor homogenization temperature, the model of Sterner et al. (1988). Note that slight discrepancies exist between the latter model and salinity estimated using EoS of Driesner and Heinrich (2007), but for compatibility with previous measurements, the Sterner et al. (1988) EoS is implemented here;
- For halite melting at temperatures greater than the liquid + vapor phase homogenization temperature, the model of Lecumberri-Sánchez et al. (2012).

3. Outline and description of the program *ProBrine*

The preceding subsections listed the key phase equilibria, thermodynamic and transport properties of the system H_2O -NaCl, along with the selected numerical models that can be used to calculate these properties. In order to implement the new comprehensive model, these models were assembled and programmed in Microsoft Visual Basic for Applications in Excel (Appendices 1–4). The end result is the program *ProBrine*, capable of evaluating fluid phase equilibria, interpreting microthermometric results, and analyzing quantitatively all of the

aforementioned properties of the H_2O -NaCl system. Different parts of the *ProBrine* program have slightly different *PT* constraints: 1) phase equilibria operates in range from 0 to 1000 °C and from 0 to 5000 bar; 2) volumetric and thermodynamic properties are valid in *PT* range from 0 to 1000 °C and from 1 to 5000 bar; 3) salinity of fluid inclusions can be estimated at temperatures above –21.2 °C.

The program has been deliberately designed for flexibility in terms of desired input and output variables, as well as in terms of incorporating datasets or running simulations. As such, the basic structure of the code is rooted in user-defined functions that can be run either directly in Microsoft Excel using the standard syntax of Excel formulae, through VBA by executing as a macro, or by using the provided graphical user interface (GUI, Fig. 3A). A non-exhaustive list of the user-defined functions and their input/output parameters are provided in Table 1. Note that the GUI was developed for PCs and is not fully supported for Mac users, but all the same functionality can be accessed through the user-defined functions (Table 1). The GUI (Fig. 3) is designed to estimate properties in isothermal (P_x), isobaric (T_x) and constant salinity (PT) cross sections, as well as in three-dimensional PTx space. The program is included in Appendix 1, and detailed descriptions of its graphical user interface, functions and structure of the code are provided in Appendix 2.

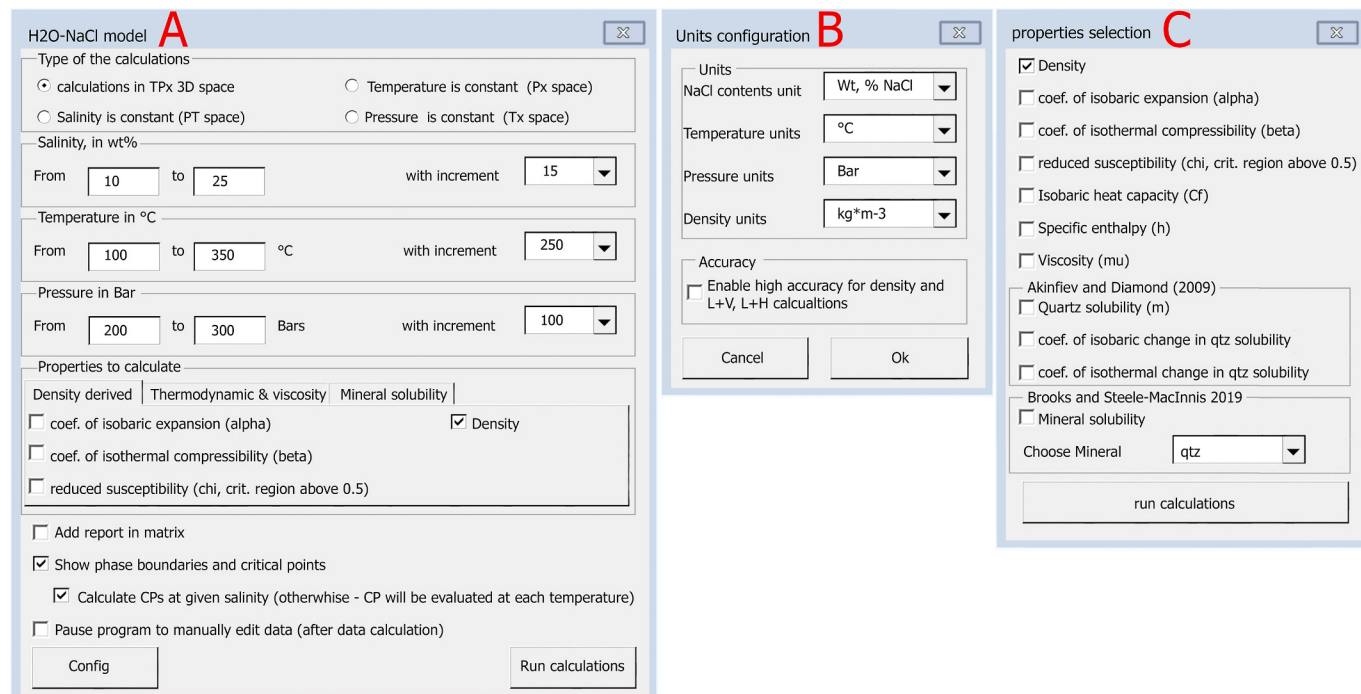


Fig. 3. Screenshots demonstrating a graphical user interface (GUI) of the *ProBrine* program. 2A shows the main window, 2B – units configuration window, which appears either by clicking “Config” button in main window (A), or by running program through user input via “Read from the page” button on the “model” sheet. The window shown on 2C is a property selector, appearing after the units configuration, if “Read from the page” run is initiated.

3.1. Example applications

3.1.1. Calculating phase equilibria and fluid properties

Depending on the PTx coordinates, H_2O -NaCl fluids may consist of a liquid, vapor or halite phases simultaneously or any combination of these three. To evaluate which set of phases is present at given coordinates, the pressure, temperature and composition of the point should be compared against PTx coordinates of halite solidus, vapor-saturated halite, vapor-saturated liquid and liquid-saturated vapor fields (Fig. 1, L + H, V + H, L + V). We emphasize that while pressure limits for phase equilibria of Driesner and Heinrich (2007) EoS are defined between 0 and 5000 bar, the lower pressure limit for fluid properties in most of the EoS are set to 1 bar. This imposes a relatively trivial constraint for the aforementioned properties, which cannot be evaluated if the pressure is below 1 bar.

The *ProBrine* program includes functionality to determine the stable phase state at a given PTx point, as well as to define the coordinates of the enclosing phase boundaries along isothermal, isobaric or iso-compositional sections through PTx space. An example calculation of this type is shown in Fig. 2. A PTx point with a salinity of 30 wt% NaCl, at 600 °C and 500 bar (Fig. 2B, C, dark point) is constrained within the liquid and vapor field. The vapor-saturated liquid pressure for 30 wt% NaCl and 600 °C is 891 bar, and the halite-saturated vapor field is limited at 390 bar (Fig. 2B). The salinity of the vapor at liquid-saturated surface is 0.25 wt% NaCl, while the salinity of the liquid phase at vapor-saturated is 65.6 wt% NaCl at 600 °C and 500 bar.

For the single-phase fluid, we can evaluate volumetric and thermodynamic properties. For example, the fluid with salinity of 15 wt% NaCl, at 450 °C and 1500 bar (Fig. 4A, gray point) will have a density of 0.836 g/cm³, an isochore at this point with a slope of 11.58 bar/°C, and isobaric heat capacity of ~3.6 kJ/(kg K).

3.1.2. Plotting phase diagrams

Phase diagrams can be generated in three-dimensional PTx space (Fig. 2A), or as two-dimensional slices at constant salinity (PT), isothermal (Px) or isobaric (Tx) conditions (Fig. 2B-2D). The latter two-

dimensional phase diagrams are the special cases of three-dimensional PTx space, with one parameter held constant. Here we provide an example of how to generate three-dimensional PTx phase diagram, similar to that shown in Fig. 2A. Each point populating the liquid-saturated halite, vapor-saturated halite, vapor-saturated liquid, and liquid-saturated vapor surfaces can be estimated as described in section 4.1.1.

A liquid-saturated halite surface is constrained by the halite melting curve at $T \geq T_{NaCl}^{triple}$ (800.7 °C) with a salinity of pure NaCl. A lower pressure-temperature limit of a liquid-saturated halite surface follows the surface along which liquid + vapor + halite coexists. The same surface defines an upper pressure limit for the vapor + halite field. At lower pressures and/or salinities, the vapor + halite curve is controlled by the vapor-saturated halite surface and by the halite sublimation curve.

The liquid + vapor surface is limited in its crest by either the boiling curve of H_2O at $T \leq T_{H2O}^{CP}$ (373.946 °C), or by the locus of critical points (Fig. 2A, blue and green lines). Additionally, the crest separates the vapor-saturated liquid subsurface from the liquid-saturated vapor. The low-pressure limit for both of these surfaces is controlled by the intersection with the surface of coexisting liquid + vapor + halite phases at $T \leq T_{NaCl}^{triple}$ (800.7 °C), and at higher temperatures by the halite boiling curve.

3.1.3. Interpretation of fluid-inclusion data

Microthermometric data obtained during heating runs are used to identify the salinity and minimum temperature at which the fluid inclusions were trapped. During these runs, the observer will note the melting temperature (T_m) of the phase, the identity of the solid phase (either ice, hydrohalite or halite), and homogenization temperature (T_H). The homogenization temperature is defined as the temperature of disappearance of either the vapor phase (bubble disappearance) or the liquid phase (expansion of the bubble to fill the inclusion), or fading of the meniscus between liquid and vapor (critical phenomenon) during heating. We note that phase transition of liquid + halite to liquid by melting halite in the absence of vapor (i.e., L + H to L) can be defined as both melting and “homogenization” to single phase, but we refer to

Table 1

Description of functions, designed for generating data.

Function name	Arguments (see table footnotes)	Returned units	Description of function, superscript indicate references, provided in footnotes
Brine_Density	x, T, P, \odot	kg/m ³	Returns the density of H ₂ O-NaCl, Eq. (7) ^a
Brine_dP_dT_for_Isochore	x, T, P, ρ	Bar/K	Returns slope of the isochore at given parameters
Brine_Enthalpy	x, T, P, \odot	J/kg	Returns the specific enthalpy of H ₂ O-NaCl, Eq. (21) ^a
Brine_Isobaric_Expanisivity_alpha	x, T, P, ρ, \odot	1/K	Returns the isobaric expansivity coefficient (α) Eq. (8) ^b
Brine_Isobaric_heat_caps	x, T, P, \odot	J/(kg·K)	Returns the isobaric heat capacity of H ₂ O-NaCl Eq. (27) ^a , divided by (1 + X_{NaCl}) where X_{NaCl} is a molar fraction. This term was omitted in original publication but should be used, according to personal communications with Thomas Driesner.
Brine_Isothermal_Compressibility_beta	x, T, P, ρ, \odot	1/bar	Returns the isothermal compressibility (β) Eq. (7) ^b
Brine_Viscosity	x, T, P	μPas	Returns the viscosity of H ₂ O-NaCl single phase mixture, Eq. (3) ^c
Brine_Xsi_Critical_Region	$x, T, P, \rho, \beta, \odot$	N/A	Returns the reduced susceptibility parameter, indicating critical region limits at value of 0.5, eq. in Section 2.2.3. ^d
IAPWS_Water_Density	T, P, \odot	kg/m ³	Returns the density of pure H ₂ O according to IAPWS-95 formulation ^e . Root finding algorithms applied to eq. for H ₂ O pressure at given temperature and density, in Table 6.3
IAPWS_Water_Enthalpy	T, ρ	J/kg	Returns the specific enthalpy of H ₂ O, calculated according to IAPWS-95 formulation ^e , eq. in Table 6.3
IAPWS_Water_Isob_heat_capacity	T, ρ	J/(kg·K)	Returns the isobaric heat capacity of H ₂ O, calculated according to IAPWS-95 formulation, eq. in Table 6.3 ^e
IAPWS_Water_Isochoric_heat_capacity	T, ρ	J/(kg·K)	Returns the isochoric heat capacity of H ₂ O, calculated according to IAPWS-95 formulation, eq. in Table 6.3 ^e
IAPWS_Water_Pressure	T, ρ	Bar	Returns the pressure of H ₂ O at given conditions, according to IAPWS-95 formulation, eq. in Table 6.3 ^e
IAPWS_Water_Liq_Dens_V_sat	T	kg/m ³	Returns the vapor-saturated liquid density of pure H ₂ O according to IAPWS-95 formulation, Eq. (2.6) ^e
IAPWS_Water_Vap_Dens_L_sat	T	kg/m ³	Returns the liquid-saturated vapor density of pure H ₂ O according to IAPWS-95 formulation, Eq. (2.7) ^e
IAPWS_Water_Viscosity	T, ρ	μPas	Returns the dynamic viscosity of pure H ₂ O according to the IAPWS Formulation 2008, extending IAPWS-95, Eq. (2) ^f
Phases_PTx_Surveyor	x, T, P	text	Checks the state of the fluid for a given PTx point, or estimates coexisting phase along the lines of provided PT, Px, Tx coordinates (at least 2 parameters are required) ^{g,h}
Phases_x_Halite_Liquidus	T, P	x	Returns the concentration for halite liquidus at given pressure and temperature, Eq. (8) ^g
Phases_x_Halite_saturated_vapor	T, P	x	Returns the concentration for halite-saturated vapor at given pressure and temperature, Eq. (9) ^g
Phases_P_crit	T	Bar	Returns the critical pressure at given temperature, Eqs. (5) and (7) ^g
Phases_P_Halite_Boil	T	Bar	Returns the pressure of the halite boiling at given temperature, Eq. (3) ^g
Phases_P_Halite_SUBL	T	Bar	Returns the pressure of the halite sublimation at given temperature, Eq. (2) ^g
Phases_P_LVH_Coexistence	T	Bar	Returns the pressure (bar) of liquid-vapor-halite coexisting curve for given temperature, Eq. (10) ^g
Phases_T_Halite_Melting	P	°C	Returns the temperature of halite melting, Eq. (1) ^g
Phases_x_crit	T	x	Returns the concentration for critical point at given temperature, Eqs. (5) and (7) ^g
Phases_x_of_coexisting_phases	x, T, P	text	Returns the salinity for coexisting phases, if the fluid is in two phase fluid state, Eqs. (8), (11), (12) ^g
Phases_x_VL_coex_Liquid_side	T, P	x	Returns the concentration of liquid-vapor coexistence surface at liquid branch, for given temperature and pressure, Eq. (12) ^g
Phases_x_VL_coex_Vapor_side	T, P	x	Returns the concentration of liquid-vapor coexistence surface at vapor branch, for given temperature and pressure, Eq. (11) ^g
Phases_Single_ph_pressure_at_TX	x, T	Bar	Returns the L + V pressure at the point of interest ^g
SiO2_isobaric_change_solubility	x, T, P, ρ	1/K	Returns the coefficient of isobaric change in SiO ₂ solubility, Eq. (12) ^b
SiO2_isothermal_change_solubility	x, T, P, ρ	1/bar	Returns the coefficient of isothermal change in SiO ₂ solubility, Eq. (11) ^b
SiO2_solubility	x, T, P, ρ	Molal	Returns the SiO ₂ solubility in fluid, Eq. (10) ^h
Mineral_Solubility	$x, T, P, \rho, \text{MinID}$	Molal	Returns the mineral solubility, for quartz, calcite, corundum, fluorapatite, fluorite and rutile ⁱ
FlInclusion_Salinity	T_m, T_H, PhID	x	Returns salinity of the fluid inclusion. If PhID is omitted, then salinity estimated based on ice melting. Depending on the input values, salinity estimated according to one of models ^{j,k,l}
S_Unit_Converter	#, X_in, X_out		Converts salinity between different units. If incoming value expressed in percent (0–100). Returning values are in fraction, ranged from 0 to 1.

Abbreviations: x is weight percent of NaCl, ranged from 0 to 100; T – temperature in degrees Celsius, T_m and T_H refer to temperatures of melting of phase PhID (ice, hydrohalite, halite) and homogenization by disappearance of the bubble; P – pressure in bar; ρ – density of the fluid, in kg/m³, estimated by using appropriate function (either Brine_Density or IAPWS_Water_Density); β – isothermal compressibility coefficient of fluid at given composition; \odot - true/false variable to enable/disable high precision in evaluation of density or phase boundaries; MinID – mineral identifier, for which mineral solubility needs to be evaluated. Supports the following minerals: fluorapatite (ap), calcite (calc), corundum (cor), fluorite (fl), quartz (qtz) and rutile (ru); PhID – daughter phase identifier, melted in the fluid inclusion. Can be either halite (h), hydrohalite (hh) or ice (i); # - incoming number; X_in and X_out can be expressed in weight (“WtPer”), molar (“MolPer”), volume (“VolPer”) percent, as well as molality (“Molal”) Mol/kg_{H2O}.

^a (Driesner, 2007).^b (Klyukin et al., 2016).^c (Klyukin et al., 2017).^d (Anisimov et al., 2004).^e (Wagner and Prüß, 2002).^f (Huber et al., 2009).^g (Driesner and Heinrich, 2007).^h (Akifiev and Diamond, 2009).ⁱ (Brooks and Steele-MacInnis, 2019).^j (Bodnar, 1993).^k (Sternert et al., 1988).^l (Lecumberri-Sanchez et al., 2012).

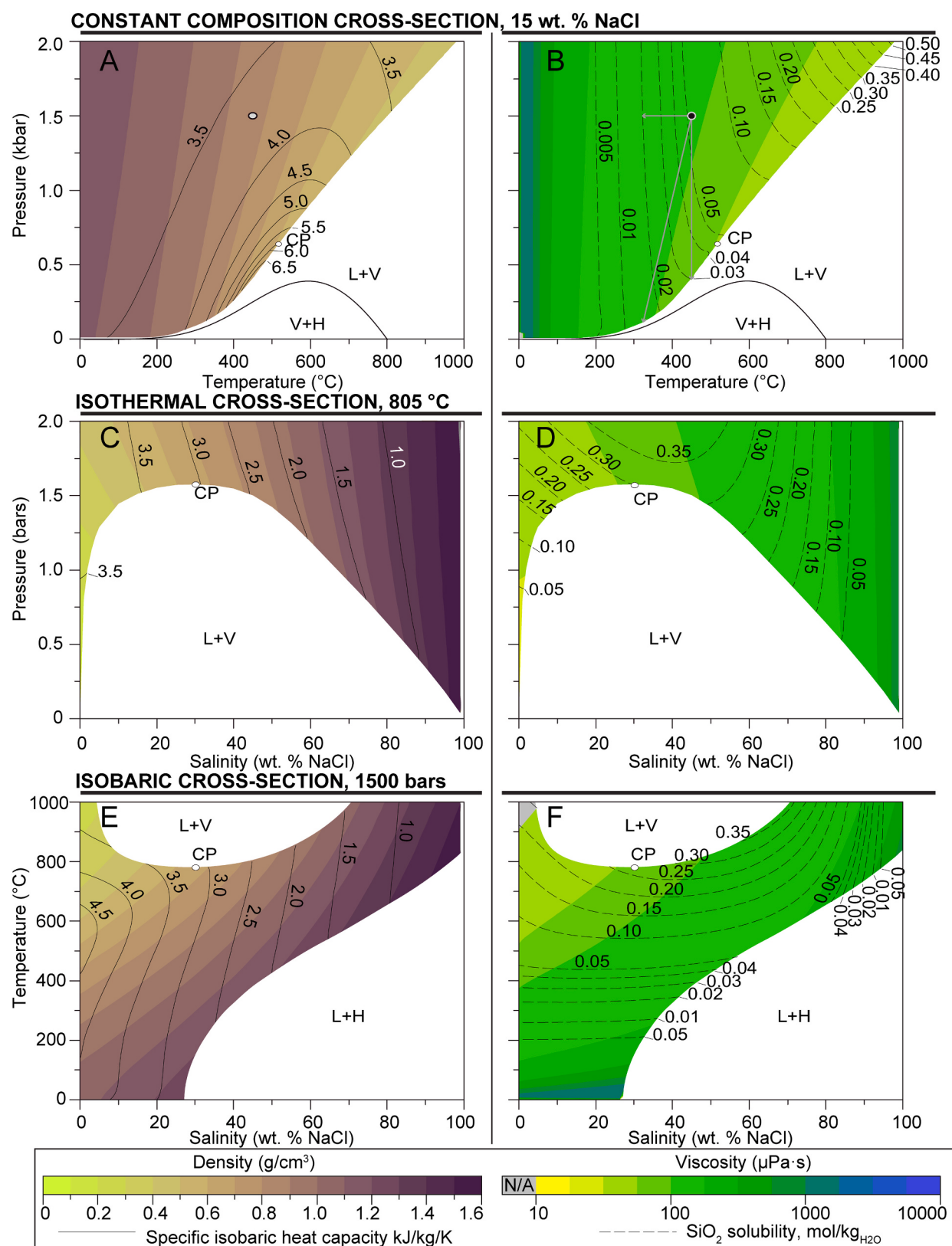


Fig. 4. Cross sections, with property calculations, at constant salinity of 15 wt% NaCl (A, B), isothermal at 805 °C (C, D), isobaric at 1500 bar (E, F). Left diagrams (A, E) show density variation (in color) and specific isobaric heat capacity (thin solid lines). Diagrams on the right side (B, D, F) show viscosity (in color) and SiO₂ solubility (thin dashed lines). Calculations performed using the graphic user interface (GUI).

this process strictly as melting to avoid ambiguity in describing phase transitions $L + H + V$ to $L + V$ versus $L + H$ to L . These parameters (T_m , the solid phase that has melted at T_m , T_H , and mode of T_H) are combined to identify the salinity, bulk density, the PTx point at which the isochore with bulk density originates (or minimum trapping conditions), and the slope of the isochore.

Salinity determination is based on a few various models, depending on the melting phase (i.e. ice, hydrohalite or halite), and the relation between T_H and T_m :

- In the case of ice melting, the model of Bodnar (1993) is used. For example, at $T_m = -5^\circ\text{C}$ salinity is estimated as 7.9 wt% NaCl.
- In the case of observed hydrohalite dissolution, or halite melting at temperatures $T_m \leq T_H$, the model of Stern et al. (1988) is used. For example, at $T_m = -5^\circ\text{C}$ of the hydrohalite, salinity would be estimated as 25.6 wt% NaCl. We note here, that the hydrohalite melting curve has a high Tx slope, which results in relatively small differences in salinity over the temperature range of hydrohalite melting (23.5 to 26.2 wt% NaCl). But if hydrohalite melting is observed, its T_m temperature allows better salinity identification compared to assigning an average salinity of 24.7 wt% NaCl, and this may play an important role in describing fluid inclusion assemblages.
- In the case of $T_m > T_H$ we adopted the model of Lecumberri-Sánchez et al. (2012). For the case $T_m = 250^\circ\text{C}$ and $T_H = 220^\circ\text{C}$, salinity is estimated to be 35.0 wt% NaCl.

As an example, we will use the hypothetical case of a fluid trapped in a mineral collected from a Mid-Ocean Ridge hydrothermal vent system at conditions of hydrostatic pressure of 3 km depth below the surface (Fig. 5). The ice melting temperature $T_m = -5^\circ\text{C}$ yields a salinity of 7.9 wt% NaCl. The fluid inclusion homogenizes to liquid at $T_H = 250^\circ\text{C}$. Knowing the T_H and salinity provides pressure, corresponding to conditions at which the vapor-saturated surface has a salinity of 7.9 wt% NaCl and temperature of 250 °C (homogenization pressure $P_H = 38.0$ bar). Salinity, T_H , and P_H yield bulk density of the fluid inclusion (0.87 g/cm^3), for which we can identify the slope of the isochore ($\sim 14.5 \text{ bar}/^\circ\text{C}$). The isochore originated from the $T_H P_H x$ point intersects our hypothetical pressure constraint of 3 km (or 300 bar, assuming hydrostatic gradient) at 269 °C.

3.1.4. Fluid inclusion heating path

The program ProBrine has been used to evaluate volumetric properties, salinity, and phase ratio of vapor, liquid, and halite for fluid inclusions during heating from room temperature to total homogenization. Coexisting phases in the fluid inclusions during heating/cooling experience complex, reversible changes, in which the only

relative changes in phase ratio can be directly observed. Nevertheless, fluid inclusions can be described as a closed system: the bulk volume and mass, summed over all phases, remain constant during microthermometry. In addition to that we assume that all present phases in fluid inclusions are in equilibrium, and obey PTx constraints emplaced by phase equilibria. Therefore, at any $T < T_H$ we can calculate salinity and density of each phase, which yields the mass and volume for every phase that is present. For exact calculation procedure, discussion, and extensive result presentation we reference the work of Klyukin et al. (2019).

Here we review an example case of a fluid inclusion with a salinity of 5 wt% NaCl, homogenizing at critical temperature and pressure (422.1°C , 337.14 bar, bulk density $\sim 0.486 \text{ g/cm}^3$). For this fluid inclusion, critical homogenization behavior is observed: upon homogenization, the meniscus separating vapor and liquid phases gradually fades, until the distinction between liquid and vapor ceases to exist and the inclusion homogenizes at the critical temperature and pressure. Upon cooling below the homogenization temperature, the single-phase fluid splits into vapor and liquid phases. Close to the homogenization temperature, at 420°C , the vapor phase occupies $\sim 12\%$ of the inclusion volume, contains 2.6 wt% NaCl salinity and has a density of 0.392 g/cm^3 . The remaining volume is occupied by a liquid phase that has 5.3 wt% NaCl salinity and density of 0.488 g/cm^3 . Similar calculations repeated at 100, 200, 300 and 400°C indicate that vapor phase volume changes non-linearly, (51, 47, 40, 25 vol%) and accelerates at temperatures approaching homogenization. The change in volume occupied by a vapor phase as temperature approaches the T_H masks behavior of the fluid inclusion homogenizing to a liquid phase, therefore such fluid inclusions may be misinterpreted as homogenizing to the liquid.

3.1.5. Simulating changes in mineral solubility on a cooling or decompression path

Mineral solubility changes non-linearly in response to changes in PTx conditions. The program ProBrine provides tools to estimate the solubility of quartz according to the model of Akinfiev and Diamond (2009), and solubilities of quartz, calcite, corundum, fluorapatite, fluorite, and rutile using the model of Brooks and Steele-MacInnis (2019). In this section, we describe an example of how quartz solubility changes during isothermal decompression, and isobaric/isochoric cooling. Both aforementioned models yield nearly the same solubility for quartz, and results reported below are estimated using the model of Brooks and Steele-MacInnis (2019).

A hydrothermal fluid with salinity of 15 wt% NaCl, trapped at 450°C and pressure of 1500 bar has a quartz solubility of $0.054 \text{ mol/kg}_{\text{H}_2\text{O}}$ (Fig. 4B, dark dot) Assuming isochoric cooling to the vapor-saturated liquid surface which occurs at 325°C and 111 bar, quartz

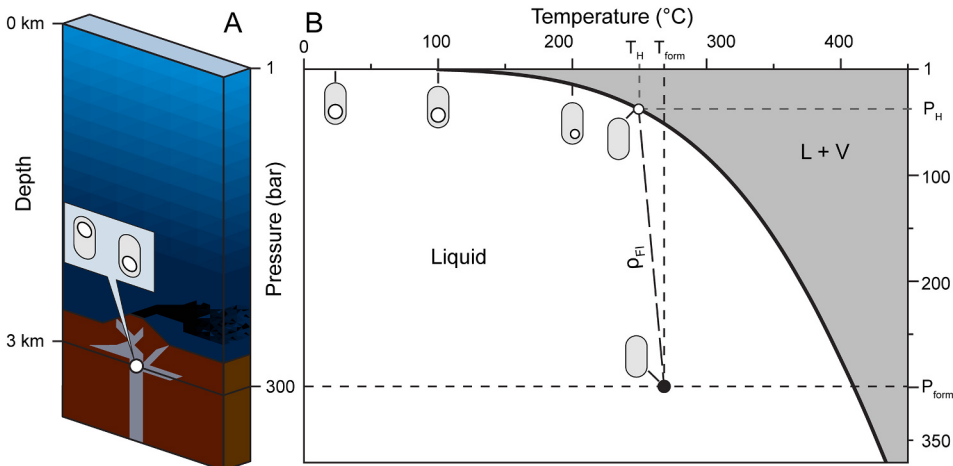


Fig. 5. Schematic cross section of a subseafloor hydrothermal system with fluid inclusions trapped at depth of 3 km (A). These fluid inclusions have homogenization temperature T_H of 250°C and ice melting temperature T_{ICE} of -5°C , which corresponds to salinity of 7.9 wt% NaCl. Pressure-temperature phase diagram (B) for salinity of 7.9 wt% NaCl demonstrate how fluid inclusions measurements can be interpreted to identify formation pressure and temperature (P_{form} and T_{form}): for given T_H and salinity, the homogenization pressure P_H is constrained. $T_H P_H x$ provides bulk density of the fluid inclusion and slope of the isochore that originates from $T_H P_H$ and intersects the pressure constraint at a formation temperature of 269°C .

solubility drops to 0.014 mol/kg_{H2O}. In the case of Isothermal decompression down to the vapor-saturated liquid surface (1500 bar, and 408 bar) quartz solubility decreases to 0.03 mol/kg_{H2O}. Isobaric cooling from 450 to 325 °C reduces quartz solubility to 0.019 mol/kg_{H2O}. Thus, the quartz solubility drops by ~75% following the isochore, by 45% for isothermal decompression and by 65% for isobaric cooling.

3.2. Comparison with previous numerical models

The program described here offers a number of unique advantages compared to existing models. MacFlinCor (Brown and Hagemann, 1995) provides a wide range of tools for several binary, ternary and multicomponent systems, but the program has not been updated in light of more recent equations of state, and does not operate on modern computers. The program implementing the model of Duan et al. (1995) similarly has not been updated and available versions are only pre-compiled executables with limited functionality that cannot be modified or expanded. The SoWat package (Driesner and Heinrich, 2007; Driesner, 2007) is organized into three separate programs: one to evaluate the fluid inclusion composition; one to calculate isothermal or isobaric cross sections; and one to estimate fluid composition at a given *PTx* point. The program AqSo_NaCl (Bakker, 2018, 2019) is designed to evaluate fluid properties at specific *PTx* conditions or fluid inclusion properties. The program HokieFlincs (Steele-MacInnis et al., 2012b) was written as a Microsoft Excel spreadsheet, allowing users to interpret large datasets, but only for fluid inclusions measurements.

Compared to these aforementioned, existing programs, the one described here offers significantly more functionality and flexibility, as well as being released entirely open source for freedom to modify, copy, and build on the code. The program operates as an extension for widely spread Microsoft Excel, and can be run using the GUI or by the user-defined functions. The GUI provides a quick way to estimate properties at any given *PTx* range, and to create phase diagrams (Figs. 1, 2, 4, 5). The function input expands this functionality further, allowing users to decide on input and output parameters, to run simple numerical simulations (e.g., decompression or cooling paths), as well as to interpret data from microthermometry. For the open source release, the code is stored in the Excel workbook available in Appendix 1, and can be accessed using built-in MS Excel Integrated Development Environment. The code is freely available to review, copy, modify, expand and improve. The program structure is outlined in Appendices 2 and 3, Appendix 4 provide with example on how to use *ProBrine* to evaluate phase equilibria of the H₂O-NaCl.

Supplementary data to this article can be found online at <https://doi.org/10.1016/j.chemgeo.2020.119840>.

Declaration of competing interest

The authors declare that they have no known competing financial interests or personal relationships that could have appeared to influence the work reported in this paper.

Acknowledgments

This work was supported by the NSERC through a Discovery Grant to M.S.-M. We gratefully acknowledge Luca Fedele, Lowell Moore and Fernando Tornos for testing and feedback regarding model performance.

References

- Akinfiev, N.N., Diamond, L.W., 2009. A simple predictive model of quartz solubility in water-salt-CO₂ systems at temperatures up to 1000 °C and pressures up to 1000 MPa. *Geochim. Cosmochim. Acta* 73 (6), 1597–1608. <https://doi.org/10.1016/j.gca.2008.12.011>.
- Anderko, A., Pitzer, K.S., 1993. Equation-of-State representation of phase-equilibria and volumetric properties of the system NaCl-H₂O above 573 K. *Geochim. Cosmochim. Acta* 57 (8), 1657–1680. [https://doi.org/10.1016/0016-7037\(93\)90105-6](https://doi.org/10.1016/0016-7037(93)90105-6).
- Anisimov, M.A., Sengers, J.V., Levelt Sengers, J.M.H., 2004. Near-critical behavior of aqueous systems. In: Palmer, D.A., Fernandez-Prini, R., Harvey Allan, H. (Eds.), *Aqueous Systems at Elevated Temperatures and Pressures: Physical Chemistry in Water, Steam and Hydrothermal Solutions*. Elsevier Ltd, Amsterdam, pp. 29–72. <https://doi.org/10.1016/B978-012544461-3/50003-X>.
- Bakker, R.J., 2018. AqSo_NaCl: computer program to calculate pTVx properties in the H₂O-NaCl fluid system applied to fluid inclusion research and pore fluid calculation. *Comput. Geosci.* 115, 122–133. <https://doi.org/10.1016/j.cageo.2018.03.003>.
- Bakker, R.J., 2019. Package fluids. Part 5: the NaCl-H₂O system in fluid inclusion research and applications of the software AqSo_NaCl (Bakker, 2018). *Chem. Geol.* 525, 400–413. <https://doi.org/10.1016/j.chemgeo.2019.07.041>.
- Bischoff, J.L., Rosenbauer, R.J., 1988. Liquid-vapor relations in the critical region of the system NaCl-H₂O from 380 to 415 °C: a refined determination of the critical point and two-phase boundary of seawater. *Geochim. Cosmochim. Acta* 52 (8), 2121–2126. [https://doi.org/10.1016/0016-7037\(88\)90192-5](https://doi.org/10.1016/0016-7037(88)90192-5).
- Bodnar, R.J., 1993. Revised equation and table for determining the freezing-point depression of H₂O-NaCl solutions. *Geochim. Cosmochim. Acta* 57 (3), 683–684. [https://doi.org/10.1016/0016-7037\(93\)90378-A](https://doi.org/10.1016/0016-7037(93)90378-A).
- Bodnar, R.J., Burnham, C.W., Sternier, S.M., 1985. Synthetic fluid inclusions in natural quartz. III. Determination of phase equilibrium properties in the system H₂O-NaCl to 1000°C and 1500 bars. *Geochim. Cosmochim. Acta* 49 (9), 1861–1873. [https://doi.org/10.1016/0016-7037\(85\)90081-X](https://doi.org/10.1016/0016-7037(85)90081-X).
- Bowers, T.S., Helgeson, H.C., 1983. Calculation of the thermodynamic and geochemical consequences of nonideal mixing in the system H₂O-CO₂-NaCl on phase-relations in geologic systems - equation of state for H₂O-CO₂-NaCl fluids at high-pressure and temperatures. *Geochim. Cosmochim. Acta* 47 (7), 1247–1275. [https://doi.org/10.1016/0016-7037\(83\)90066-2](https://doi.org/10.1016/0016-7037(83)90066-2).
- Brooks, H.L., Steele-MacInnis, M., 2019. A Model for the Solubility of Minerals in Saline Aqueous Fluids in the Crust and Upper Mantle. *Am. J. Sci.* 319, 754–787. <https://doi.org/10.2475/09.2019.02>.
- Brown, P.E., Hagemann, S.G., 1995. MacFlinCor and its application to fluids in archean lode-gold deposits. *Geochim. Cosmochim. Acta* 59 (19), 3943–3952. [https://doi.org/10.1016/0016-7037\(95\)00254-W](https://doi.org/10.1016/0016-7037(95)00254-W).
- Coogan, L.A., Seyfried, W.E., Pester, N.J., 2019. Environmental controls on mid-ocean ridge hydrothermal fluxes. *Chem. Geol.* 119285. <https://doi.org/10.1016/j.chemgeo.2019.119285>.
- Coumou, D., Driesner, T., Heinrich, C.A., 2008. The structure and dynamics of mid-ocean ridge hydrothermal systems. *Science* 321 (5897), 1825–1828. <https://doi.org/10.1126/science.1159582>.
- Driesner, T., 2007. The system H₂O-NaCl. II. Correlations for molar volume, enthalpy, and isobaric heat capacity from 0 to 1000 °C, 1 to 5000 bar, and 0 to 1 X-NaCl. *Geochim. Cosmochim. Acta* 71 (20), 4902–4919. <https://doi.org/10.1016/j.gca.2007.05.026>.
- Driesner, T., Heinrich, C.A., 2007. The system H₂O-NaCl. I. Correlation formulae for phase relations in temperature-pressure-composition space from 0 to 1000 °C, 0 to 5000 bar, and 0 to 1 XNaCl. *Geochim. Cosmochim. Acta* 71 (20), 4880–4901. <https://doi.org/10.1016/j.gca.2006.01.033>.
- Duan, Z., Möller, N., Wære, J.H., 1995. Equation of state for the NaCl-H₂O-CO₂ system: prediction of phase equilibria and volumetric properties. *Geochim. Cosmochim. Acta* 59 (14), 2869–2882. [https://doi.org/10.1016/0016-7037\(95\)00182-4](https://doi.org/10.1016/0016-7037(95)00182-4).
- Frank, M.R., Candela, P.A., Piccoli, P.M., 2003. Alkali exchange equilibria between a silicate melt and coexisting magmatic volatile phase: an experimental study at 800°C and 100 MPa. *Geochim. Cosmochim. Acta* 67 (7), 1415–1427. [https://doi.org/10.1016/S0016-7037\(02\)01181-X](https://doi.org/10.1016/S0016-7037(02)01181-X).
- Garven, G., 1985. The role of regional fluid flow in the genesis of the Pine Point Deposit, Western Canada sedimentary basin. *Econ. Geol.* 80 (2), 307–324. <https://doi.org/10.2113/gsecongeo.80.2.307>.
- Gottschalk, M., 2007. Equations of State for complex fluids. *Rev. Mineral. Geochem.* 65 (1), 49–97. <https://doi.org/10.2138/rmg.2007.65.3>.
- Haar, L., Gallagher, J.S., Kell, G.S., 1984. NBS/NRC steam tables: thermodynamic and transport properties and computer programs for vapor and liquid states of water in SI units. In: Hemisphere, Washington DC.
- Huber, M., Perkins, R., Laesecke, A., Friend, D., Sengers, J., Assael, M., Metaxa, I., Vogel, E., Mareš, R., Miyagawa, K., 2009. New international formulation for the viscosity of H₂O. *J. Phys. Chem. Ref. Data* 38 (2), 101–125.
- Jupp, T.E., Schultz, A., 2000. A thermodynamic explanation for black smoker temperatures. *Nature* 403 (6772), 880–883. <https://doi.org/10.1038/35002552>.
- Jupp, T.E., Schultz, A., 2004. Physical balances in seafloor hydrothermal convection cells. *Journal of Geophysical Research: Solid Earth* 109 (B5), B05101. <https://doi.org/10.1029/2003JB002697>.
- Kesler, S.E., 2005. Ore-forming fluids. *Elements* 1 (1), 13–18. <https://doi.org/10.2113/gselements.1.1.13>.
- Klyukin, Y.I., Driesner, T., Steele-MacInnis, M., Lowell, R.P., Bodnar, R.J., 2016. Effect of salinity on mass and energy transport by hydrothermal fluids based on the physical and thermodynamic properties of H₂O-NaCl. *Geofluids* 16 (3), 585–603. <https://doi.org/10.1111/gfl.12181>.
- Klyukin, Y.I., Lowell, R.P., Bodnar, R.J., 2017. A revised empirical model to calculate the dynamic viscosity of H₂O-NaCl fluids at elevated temperatures and pressures (≤ 1000 °C, ≤ 500 MPa, 0–100 wt % NaCl). *Fluid Phase Equilib.* 433, 193–205. <https://doi.org/10.1016/j.fluid.2016.11.002>.
- Klyukin, Y.I., Steele-MacInnis, M., Lecumberri-Sánchez, P., Bodnar, R.J., 2019. Fluid inclusion phase ratios, compositions and densities from ambient temperature to homogenization, based on PVTX properties of H₂O-NaCl. *Earth Sci. Rev.* 198, 10294. <https://doi.org/10.1016/j.earscirev.2019.10294>.
- Lecumberri-Sánchez, P., Steele-MacInnis, M., Bodnar, R.J., 2012. A numerical model to

- estimate trapping conditions of fluid inclusions that homogenize by halite disappearance. *Geochim. Cosmochim. Acta* 92, 14–22. <https://doi.org/10.1016/j.gca.2012.05.044>.
- Lecumberri-Sanchez, P., Steele-MacInnis, M., Bodnar, R.J., 2015. Synthetic fluid inclusions XIX: Experimental determination of the vapor-saturated liquidus of the system H₂O-NaCl-FeCl₂. *Geochim. Cosmochim. Acta* 148, 34–49. <https://doi.org/10.1016/j.gca.2014.08.015>.
- Lecumberri-Sanchez, P., Luo, M., Steele-MacInnis, M., Runyon, S.E., Sublett, D.M., Klyukin, Y., Bodnar, R.J., 2020. Synthetic fluid inclusions XXII: Properties of H₂O-NaCl ± KCl fluid inclusions trapped under vapor- and salt-saturated conditions with emphasis on the effect of KCl on phase equilibria. *Geochim. Cosmochim. Acta* 272 (1), 78–92. <https://doi.org/10.1016/j.gca.2019.12.018>.
- Li, X.H., Klyukin, Y.I., Steele-MacInnis, M., Fan, H.R., Yang, K.F., Zoheir, B., 2020. Phase equilibria, thermodynamic properties and solubility of quartz in saline-aqueous-carbonic fluids: Application to orogenic and intrusion-related mesothermal gold deposits. *Geochim. Cosmochim. Acta* 283, 201–221. <https://doi.org/10.1016/j.gca.2020.06.008>.
- Liebscher, A., Heinrich, C.A., 2007. Fluid-fluid interactions in the Earth's lithosphere. *Rev. Mineral. Geochem.* 65 (1), 1–14. <https://doi.org/10.2138/rmg.2007.65.1>.
- Lister, C., 1995. Heat transfer between magmas and hydrothermal systems, or, six lemmas in search of a theorem. *Geophys. J. Int.* 120 (1), 45–59.
- Mao, S., Duan, Z., 2009. The viscosity of aqueous alkali-chloride solutions up to 623 K, 1,000 bar, and high ionic strength. *Int. J. Thermophys.* 30 (5), 1510–1523. <https://doi.org/10.1007/s10765-009-0646-7>.
- Miron, G.D., Wagner, T., Kulik, D.A., Heinrich, C.A., 2016. Internally consistent thermodynamic data for aqueous species in the system Na-K-Al-Si-O-H-Cl. *Geochim. Cosmochim. Acta* 187, 41–78. <https://doi.org/10.1016/j.gca.2016.04.026>.
- Monecke, T., Monecke, J., Reynolds, T.J., Tsuruoka, S., Bennett, M.M., Skewes, W.B., Palin, R.M., 2018. Quartz solubility in the H₂O-NaCl System: a framework for understanding vein formation in porphyry copper deposits. *Econ. Geol.* 113 (5), 1007–1046. <https://doi.org/10.5382/econgeo.2018.4580>.
- Norton, D.L., 1984. Theory of hydrothermal systems. *Annu. Rev. Earth Planet. Sci.* 12 (1), 155–177.
- Palliser, C., McKibbin, R., 1998a. A model for deep geothermal brines, I: T-p-X state-space description. *Transp. Porous Media* 33 (1–2), 65–80. <https://doi.org/10.1023/A:1006537425101>.
- Palliser, C., McKibbin, R., 1998b. A model for deep geothermal brines, II: thermodynamic properties – density. *Transp. Porous Media* 33 (1–2), 129–154. <https://doi.org/10.1023/A:1006597626918>.
- Palliser, C., McKibbin, R., 1998c. A model for deep geothermal brines, III: thermodynamic properties – enthalpy and viscosity. *Transp. Porous Media* 33 (1–2), 155–171.
- <https://doi.org/10.1023/A:1006549810989>.
- Roedder, E., 1972. Composition of fluid inclusions. In: United States Geological Survey Professional Paper 440-JJ.
- Roedder, E., 1984. Fluid inclusions. In: Rev. Mineral. Mineralogical Society of America, pp. 12.
- Steele-MacInnis, M., 2018. Fluid inclusions in the system H₂O-NaCl-CO₂: an algorithm to determine composition, density and isochore. *Chem. Geol.* 498, 31–44. <https://doi.org/10.1016/j.chemgeo.2018.08.022>.
- Steele-MacInnis, M., Bodnar, R.J., Naden, J., 2011. Numerical model to determine the composition of H₂O-NaCl-CaCl₂ fluid inclusions based on microthermometric and microanalytical data. *Geochim. Cosmochim. Acta* 75 (1), 21–40. <https://doi.org/10.1016/j.gca.2010.10.002>.
- Steele-MacInnis, M., Han, L., Lowell, R.P., Rimstidt, J.D., Bodnar, R.J., 2012a. The role of fluid phase immiscibility in quartz dissolution and precipitation in sub-seafloor hydrothermal systems. *Earth Planet. Sci. Lett.* 321–322, 139–151. <https://doi.org/10.1016/j.epsl.2011.12.037>.
- Steele-MacInnis, M., Lecumberri-Sanchez, P., Bodnar, R.J., 2012b. HokieFlincs_H₂O-NaCl: a Microsoft Excel spreadsheet for interpreting microthermometric data from fluid inclusions based on the PVTX properties of H₂O-NaCl. *Comput. Geosci.* 49, 334–337. <https://doi.org/10.1016/j.cageo.2012.01.022>.
- Steele-MacInnis, M., Ridley, J., Lecumberri-Sanchez, P., Schlegel, T., Heinrich, C.A., 2016. Application of low-temperature microthermometric data for interpreting multicomponent fluid inclusion compositions. *Earth Sci. Rev.* 159, 14–35. <https://doi.org/10.1016/j.earscirev.2016.04.011>.
- Sternert, S.M., Hall, D.L., Bodnar, R.J., 1988. Synthetic fluid inclusions. V. Solubility relations in the system NaCl-KCl-H₂O under vapor-saturated conditions. *Geochim. Cosmochim. Acta* 52 (5), 989–1005. [https://doi.org/10.1016/0016-7037\(88\)90254-2](https://doi.org/10.1016/0016-7037(88)90254-2).
- Valyashko, V.M., 2008. *Hydrothermal Properties of Materials. Hydrothermal Experimental Data*. Wiley.
- Wagner, W., Prüß, A., 2002. The IAPWS formulation 1995 for the thermodynamic properties of ordinary water substance for general and scientific use. *J. Phys. Chem. Ref. Data* 31 (2), 387–535. <https://doi.org/10.1063/1.1461829>.
- Weis, P., 2015. The dynamic interplay between saline fluid flow and rock permeability in magmatic-hydrothermal systems. *Geofluids* 15 (1–2), 350–371. <https://doi.org/10.1111/gfl.12100>.
- Weis, P., Driesner, T., Coumou, D., Geiger, S., 2014. Hydrothermal, multiphase convection of H₂O-NaCl fluids from ambient to magmatic temperatures: a new numerical scheme and benchmarks for code comparison. *Geofluids* 14 (3), 347–371. <https://doi.org/10.1111/gfl.12080>.